Light ion irradiation of Co/Pt systems: Structural origin of the decrease in magnetic anisotropy

T. Devolder*
Institut d'Electronique Fondamentale, UMR CNRS 8622, Université Paris Sud, 91405 Orsay cedex, France
(Received 16 November 1999)

We study the structural properties of Pt/Co/Pt systems submitted to He^+ ion irradiation, in order to understand why the magnetic anisotropy can be decreased in a controlled way. It is shown by grazing x-ray reflectometry that the irradiation-induced Pt and Co atom displacements can be largely accounted for by a simple ballistic recoil mechanism model. Our results indicate that even in these nm-thick films, irradiation may affect the upper and lower interfaces differently. Specifically, the upper Co interface undergoes short-range mixing, resulting in roughness, whereas the lower Co interface mostly evolves by longer-range mixing, leading to alloy formation. Irradiation also releases strain in these Co-Pt systems, but has no chemical ordering effect. Together with slow asymmetric interface roughening, the cobalt tensile strain relaxation at low fluences accounts for the magnetic anisotropy decrease. The type of analysis we propose could be useful to understand why other magnetic properties, such as interlayer exchange coupling, can be controlled by light ion irradiation.

I. INTRODUCTION

As magnetic anisotropy is due to the spin-orbit coupling,[1] it is directly related to the asymmetry of the atomic environment. The source of asymmetry may be of magnetocrystalline (lattice space group), magnetoelastic (uniaxial strain), or interfacial (symmetry breaking at interfaces) origin. Playing with these contributions has allowed the design of numerous perpendicular magnetic anisotropy (PMA) systems, a property of major interest for ultrahigh-density magnetic recording.[2,3] Among these PMA systems, Co-Pt structures have attracted considerable interest, because of a huge magnetooptical Kerr effect (MOKE) in the blue/UV spectrum.[4] In Co/Pt multilayers with small Co thickness, interface effects are strong enough to overcome the macroscopic shape anisotropy and to induce a perpendicular easy axis of magnetization.

It has recently been shown[5] that the use of controlled[6] intermixing of Co/Pt ultrathin layers via low-energy (30 keV) light ion (He^+) irradiation provides excellent control of the magnetic properties. A prerequisite for the precise tuning of magnetic properties is to use sufficiently light ions. Thus the sample atoms undergo very few short-range displacements while the ions are implanted deep into the substrate. For instance, in a Pt/Co (5 Å)/Pt sample (sputtered on glass) the coercivity (H_c) can be varied in a controlled way from 250 Oe to less than 10 Oe by adjusting the irradiation fluence, while the corresponding hysteresis loops remain square. For such an ultrathin single-layer film, irradiation also results in a Curie temperature (T_c) strong reduction, down to below room temperature at high fluence; T_c remains very precisely defined, indicating that the effects of irradiation are quite homogeneous.[7] In Co/Pt multilayers, similar fluences can also trigger a reorientation of the easy axis of magnetization from perpendicular to in plane.[5]

It has been also demonstrated that irradiation through a mask allowed sub-50-nm planar, optical-contrast-free, embedded magnetic nanostructures[8–10] to be produced. Such planar magnetically patterned films are excellent candidates for improved magnetic storage media,[11] where planarity is of paramount importance. Moreover, as anisotropy can be varied without major changes in other properties, such controllable samples are a unique model system to study the relation between structure and PMA in Pt/Co systems. Until now, however, a precise understanding of the microscopic origin of the phenomena—T_c and anisotropy decrease—is still lacking.

Here we investigate the influence of light ion irradiation on the structure of a Pt/Co (13 Å)/Pt sandwich so as to understand the tuning of its magnetic anisotropy. The cobalt thickness was chosen as the best compromise between high perpendicular anisotropy (low Co thickness) and maximum number of Co atoms in a pure Co environment. Because the characteristic ranges involved in the irradiation-induced mixing process are smaller than the cobalt layer thickness (13 Å), the precise knowledge of its structural modifications will allow to predict the behavior of any Co/Pt layered system.

Structural characterizations are performed by grazing x-ray reflectometry (GXR), a technique which is very sensitive to surface and interface roughness, layer densities, and thicknesses. Specific features were checked by atomic force microscopy (AFM) and x-ray diffraction (XRD). Magnetic characterizations rely on the polar magnetooptical Kerr effect (PMOKE) and alternative gradient field magnetometry. By comparing experiments to Monte Carlo collisional ion stopping simulations (TRIM code[12]), we show that the upper Co interfaces undergo short-range mixing, resulting in roughness increase, whereas the lower Co interface mostly evolves by longer-range mixing, leading to alloy formation. Irradiation simultaneously triggers strain release without any chemical ordering effect. Both interface roughening and tensile stress relaxation result in a lowering of the magnetic anisotropy. The analysis presented here also bears on the discussion of irradiation-induced modifications of interlayer exchange coupling.[13]

II. EXPERIMENTAL

Sample fabrication was performed through radio-frequency (rf) sputtering, using a commercial Alcatel A610

machine. The $Al_2O_3(0001)$ single-crystal substrate is first heated up to 610 °C. A 37-Å-thick Pt buffer layer is then epitaxially grown at 0.25 nm/s using dc magnetron sputtering at an argon pressure of 5×10^{-3} mbar. This gives a flat film with nearly perfect (111) texture and small (~30–40 nm) grain size. The temperature is then decreased to $T_{sub}=300$ °C. Here rf magnetron, rf diode, and again rf magnetron, respectively, are used for deposition of the 5-Å Pt underlayer and 13-Å Co and 23-Å Pt cap layers at around 0.02 nm/s. The structure of cobalt on such substrates is hexagonal compact (hcp) with (0001) orientation.[14] The irradiations were performed using an ion implanter[15] equipped with a universal medium-current ion source, providing a typical ion beam angular spread below 0.15° for the conditions used in our experiments. The ion current used here was 0.5 μA/cm^2 in order to limit sample heating below 1 K. We had previously studied the coercivity (H_c) versus ion fluence of comparable samples,[5,7] and now use these calibration values to irradiate the samples with 30-keV He^+ ions at appropriate fluences up to 3×10^{16} ions/cm^2. The different fluences were applied with a moving shutter blanking the ion flux, onto 5 $\times10$ mm^2 adjacent areas of the same initial sample, without breaking the vacuum or changing the implantation settings. Such stringent experimental conditions—identical (synchronous) sputtering conditions, equal areas—were found crucial to make very precise comparisons. The differences found in the sample structures can thus unambiguously be ascribed to the irradiation effects.

The glancing incidence reflectivity measurements were performed with a Philips X-Pert diffractometer using Cu $K\alpha$ radiation[16] ($\lambda=1.54$ Å) with incident angular divergence of 1/8° and a receiving slit of acceptance 0.1 mm. All spectra were recorded from $2\theta=1°-13°$, in 3-s steps of 0.01°. Alignment of the sample with respect to x-rays was made only once for the four different studied areas. The sample was just translated to study selectively each area. Such a procedure guarantied reproducibility of apparatus transfer function. Otherwise, some discrepancies would appear for $2\theta\leqslant3°$, due to an nonreproducible, improper elimination of the direct beam near grazing incidence and/or parasite reflections.

Magnetometry experiments were made with a homemade, standard MOKE magnetometer using He-Ne laser radiation ($\lambda=633$ nm) in the polar geometry (PMOKE). Identical field sweeping rates were used for the different studied areas. Spectroscopic MOKE measurements were performed with a commercial setup.[17]

III. RESULTS

A. Grazing x-ray reflectrometry spectra

Typical GXR spectra are shown in Fig. 1 for the as-deposited area and the highly irradiated area of the sandwich. They exhibit the classical Kiessig[18] fringes, with angular positions in close agreement with the total metallic thickness. The fringe frequency slightly decreases, while increasing the ion fluence, indicating that the metallic thickness (78 Å) has been reduced by 1.0 Å after 3×10^{16} ions/cm^2. This feature is clear when looking at the minimum of reflectivity just below 5°. As opposed to Ref. 19, in which Terris *et al.* observed a substrate thickness reduction of several ten nm after

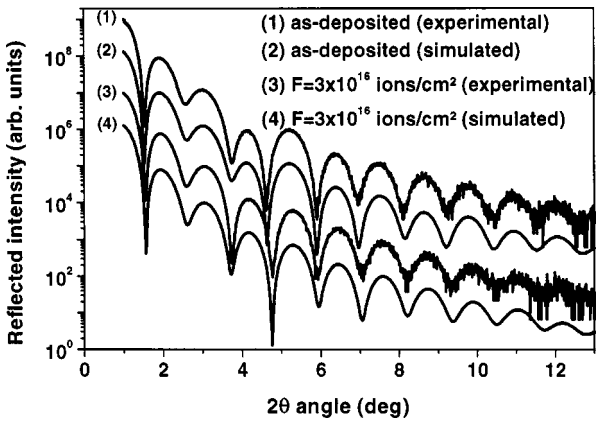

FIG. 1. Experimental and simulated GXR spectra of the as-grown area (two upper curves) and $F=3\times10^{16}$ ions/cm^2 irradiated area (two lower curves) of a Pt/Co (13 Å) /Pt sandwich. The curves are, respectively, multiplied by a factor of 1000, 100, 10, and 1.

10^{16} N^+/cm^2 (700 keV) nitrogen irradiation, our atomic force microscopy measurements indicated no shape change of our substrate. The amplitude of this difference is not understood.

The Pt (111) plane distance (d_{111}) in the sandwich was determined by $\theta/2\theta$ XRD scans (not shown). It is 2.241 Å before irradiation and decreases to 2.237 Å after the highest fluence. Such a -0.2% decrease is not sufficient to account for the sample thickness 1 Å reduction. Helium irradiation is thus likely to have a densification effect on the metallic layers. Applying the usual Sherrer formula[20] the XRD Pt(111) peak width in the $\theta/2\theta$ scans indicates that whatever the fluence, the crystallographic coherence length along Pt[111] is the full sandwich thickness.

The reflectivity mean decay between 1° and 13° follows $R\propto1/\theta^n$ for as-deposited ($n=4.8$) and highly irradiated areas ($n=4.9$), indicating negligible surface roughness ($n=4$ is expected from Fresnel equations applied to a perfectly flat surface). Damping of the Kiessig fringes is very slow: the different sandwich interfaces are well defined. The oscillation damping is slightly more pronounced in the highest-fluence case. This last point is related to a roughness increase at the Co/Pt interfaces, as will be shown below. The experimental spectra exhibit no detectable long-wavelength beating that could be associated with a surface contamination. More precisely, if there was any, its index of refraction would be very close to that of the Pt cap layer, a very unlikely case.

B. GXR simulation procedure and sample structure

More quantitative information—layer refractive index, layer thicknesses, and roughnesses—can be extracted from the data using the standard model,[21] which calculates the reflectivity curves using a recurrence based on the Fresnel equations. The parameters are the layer thicknesses and their refractive indices $n=1-\delta_n-i\beta_n$. The bulk refractive indices of Co and Pt are $\delta_{Co}=258\times10^{-7}$ and $\delta_{Pt}=550\times10^{-7}$. They follow $\delta\sim\rho Z$, where ρ is the atomic density and Z the charge number. There is little β contrast (1.4×10^{-6}) between Co and Pt, so that reasonable variation of these terms does not change the computed reflectivity spectra. Finally, the root mean square (rms) roughness of a given interface or surface can be taken into account by introducing a Debye-

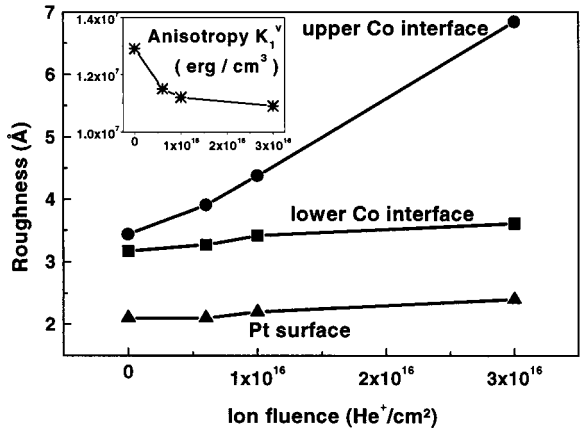

FIG. 2. Roughness of the different interfaces of a Pt/Co (13 Å) /Pt sandwich: Pt buffer/Co interface (squares), Co/Pt cap interface (circles), and Pt surface (triangles), as a function of the ion fluence. Determined from the reflectivity measurements of Fig. 1. The inset displays the value of the first-order magnetocrystalline anisotropy parameter (erg/cm^3). The correlation between roughness and magnetic anisotropy is only weak.

Waller-type factor correction of the reflected amplitude at each interface.[22] The roughness is considered as a local fluctuation of thickness. This model holds for a Gaussian distribution of local height, if the macroscopic shape fluctuations (low-momentum Fourier component of the roughness spectrum) of the sample are used as the local altitude base line.

Since the GXR spectra for different fluences are very similar (see Fig. 1), the convergence of the fit must be much better than the (small) irradiation-induced differences in the spectra. The fits are compared to the experimental data in Fig. 1. Fitting parameters are displayed in Figs. 2 and 3. Combined variations within ranges of 1% for the indices and 5% for the roughnesses did not alter significantly the experiment-fit agreement, which was excellent for all areas.

Our fitting procedure is the following.

(i) In a first step, the sandwich is divided into its nominal structure, i.e., Al_2O_3/Pt buffer (~41 Å)/Co(~13 Å)/Pt cap (~22 Å). The indices are first taken equal to that of bulk Co and Pt. Then we let the layer thicknesses vary in alternation with their refractive indices. When maximum convergence is attained, we vary independently each layer roughness. They are displayed in Fig. 2.

The sample surface remains very flat, with a roughness increase from 2.1 to 2.4 Å. This nearly constant flatness was also checked by AFM.[23] Before irradiation, the Co layer is very symmetric: the roughness of its upper and lower interfaces is 3.2 and 3.4 Å, respectively. One of our major results is that irradiation breaks this symmetry: the *upper* Co interface roughness increases at a much higher rate than that of the lower interface.[24]

To illustrate this point, we have performed a complementary set of fits. There were made by exchanging the roughnesses of upper and lower interfaces, taking the data of Fig. 2. Indices were then refitted until maximum agreement was obtained. Only weak variations (less than 1.5%) of the indices occurred. The convergence criteria of the two stratified configurations are compared in Table I. They are good in both cases,[25] but are significantly better when the greater roughness is given to the upper interface. This indicates that the roughness asymmetry is a real effect but that the roughness amplitudes should only be considered as indicative.

TABLE I. Comparison of fit convergence with the sandwich parameters of Fig. 2 (left column) and after exchange of roughness between upper and lower Co/Pt interface (right column).

Fluence (He$^+$/cm^2)	Weighted χ^2 roughnesses of Fig. 2	Weighted χ^2 exchanged roughnesses
$F=0$	6.7	8.7
$F=6\times10^{15}$	8.3	9
$F=10^{16}$	5.6	8.7
$F=3\times10^{16}$	6.8	8.4

This asymmetry is of utmost importance to understand the magnetic properties. Indeed, it has been previously assumed[5,7,19] that the irradiation-induced decrease of magnetic anisotropy could be *solely* attributed to interface roughening. The weak correlation between roughness and magnetic anisotropy variations, as sketched in Fig. 2, indicates that this statement needs to be revised. This point will be further addressed in the discussion.

Modeling of an unknown concentration gradient can be performed in two complementary ways: introducing roughness or inserting an alloy layer. In general, none is fully satisfactory. The roughness found for the upper Co/Pt interface is huge (7 Å) for the highest fluence and is no longer negligible compared to the Co layer thickness. It does not allow us to perfectly simulate the experimental data. We were consequently led to try and implement ''alloy'' layers in the simulated sandwich sample, so as to estimate the mixing phenomena that cannot be modeled by a simple roughness.

(ii) In a second step, we have thus simulated the Al_2O_3/Pt buffer (~36 Å)/Pt underlayer (~5 Å)/Co(~13 Å)/Pt overlayer (~5 Å)/Pt cap (~17 Å) structure. We have divided the Pt buffer into two parts because the dc and the 5-Å rf-sputtered Pt have *a priori* different densities and thus nonequal indices. We also divided the cap layer in two parts.[26] Such a division of the Pt layers in Co-adjacent and-nonadjacent layers enables us to distinguish between short-range and long-range effects during mixing. All layer thicknesses except the cap were kept equal to the as-deposited value, so that all the relevant information is reported in the refractive index δ. Such a fitting mode allowed us to further improve the experiment-fit accuracy, whose indices are reported in Fig. 3. The convergence was mainly limited by experimental noise at high θ. Before irradiation, the Pt buffer exhibits a gradient of refractive index: the dc and 5-Å rf-sputtered layers have different densities. As is common for sputtered layers, the dc-grown buffer layer is more dense than the (rf-grown) cap layers. Conversely, the cap layer is highly homogeneous; its division into two layers is purely artificial. Irradiation triggers a regular increase of the Co layer index and a decrease of the Pt underlayer, while all other layer indices increase smoothly. After the highest fluence, the Pt buffer and the Pt overlayer index variations bend and decrease. For the same fluence, the evolution of the Pt cap layer also slows down.

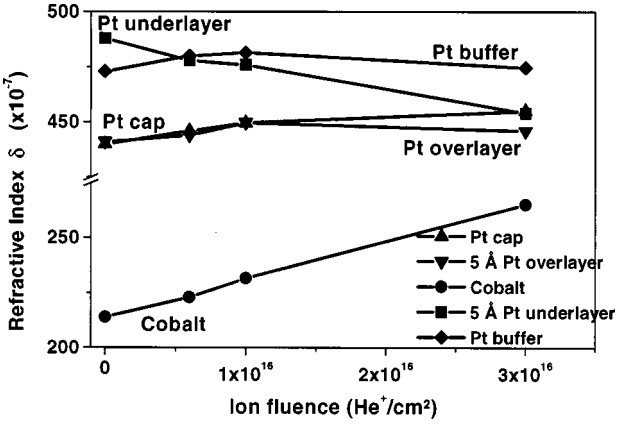

FIG. 3. Refractive indices of the different layers of a Pt/Co (13 Å) /Pt sandwich as a function of the ion fluence, determined from the reflectivity measurements of Fig. 1. Pt buffer layer (diamonds), 5-Å-thick Pt underlayer (squares) under the Co layer (circles), 5-Å Pt overlayer (down triangles), and Pt cap layer (up triangles). Vertical error bars are 1% wide.

The average index of the metallic layers increases from $\delta=420\times10^{-7}$ to $\delta=431\times10^{-7}$: the irradiation triggers a global densification.

In summary, irradiation progressively roughens the upper Co/Pt interface. The lower Pt/Co interface undergoes much less roughening but an adjacent Pt-rich layer with its own refractive index is created. At a distance greater than 5 Å apart a cobalt layer, the Pt indices indicate an irradiation-induced densification.

C. Magnetic properties

Kerr magnetooptical hysteresis loops in the perpendicular geometry are displayed in Fig. 4 in the sandwich case. Irradiation triggers an increase of the saturation Kerr rotation $\theta_K^{\max}$ from 0.141° to 0.175°. Note that measuring the Kerr effects does not give insight into the saturation magnetization M_S because the permittivity tensor is strongly function of the Co-Pt alloy concentration[17] and thus changes while irradiating. Not shown here are alternative gradient field magnetometer measurements proving indeed that the saturation magnetization M_S is constant, equal (within ±50 emu/cm^3) to that of bulk cobalt (1422 emu/cm^3).

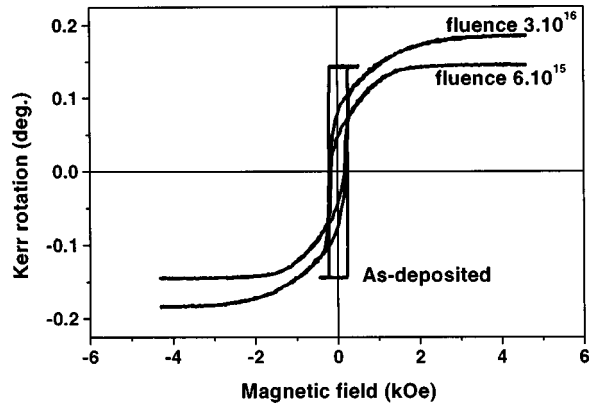

FIG. 4. PMOKE hysteresis loops of Pt/Co (13 Å) /Pt sandwich for zero fluence, 6×10^{15} and 3×10^{16}He$^+$ions/cm^2.

The as-deposited area exhibits PMA: the easy axis of magnetization is perpendicular to the layers and the loop is perfectly square. The saturation field in the hard axis loop (not shown) is ~2 kOe. Irradiated areas have their magnetization easy axis tilted towards the in-plane orientation, so that their perpendicular remnant ratios are lower than 1. Saturation of the magnetization along the perpendicular axis requires applying greater fields when increasing the ion fluence. This accounts for an irradiation-induced decrease of the magnetic anisotropy. It can be modeled by writing the total anisotropy energy as

$$E_{\text{tot}}=(-2\pi M_s^2+K_1^v)\sin^2\theta+K_2^v\sin^4\theta, \tag{1}$$

where θ is the angle between the magnetization vector and the normal to the sample surface. $-2\pi M_s^2$ is the macroscopic shape anisotropy term, whereas K_1^v and K_2^v are the first-and second-order magnetocrystalline anisotropy parameters, including the interfacial and magnetoelastic terms.

These anisotropy parameters can be computed from hard axis hysteresis loops,[27] provided the value of M_s is known. When the magnetic field is perpendicular to the sample, the energy minimization leads to

$$\frac{2[K_1^v-2\pi M_S^2]}{M_S}+\frac{4K_2^v}{M_S}\sin^2\theta=\frac{-H}{\cos\theta}. \tag{2}$$

Using $X_i=2(1-\cos^2\theta)$ and $Y_i=-HM_S/2\cos\theta$, Eq. (2) transforms into

$$Y_i=[K_1^v-2\pi M_S^2]+K_2^vX_i. \tag{3}$$

In the reversible parts of the hysteresis loops, θ does not vary from one point to another in the sample and follows $\cos\theta=\theta_K/\theta_K^{\max}$. Here X_i and Y_i can thus be computed from experimental points. A linear fit on $\{X_i,Y_i\}$ provides the anisotropy parameters. When the easy axis is perpendicular to the film, a similar procedure can be applied with the field in the plane of the sample.

The anisotropy values K_1^v are collected in Fig. 2. The decrease of K_1^v is fast until $F=6\times10^{15}$ ions/cm^2 and then goes on at a slower rate. In all areas, the second-order anisotropy parameter K_2^v is non zero: K_2^v is 0.8×10^6 erg/cm^3 before irradiation. The first fluence (6×10^{15} He$^+$/cm^2) decreases K_2^v to 0.6×10^6 erg/cm^3. It is no longer affected by further irradiation. K_2^v being nonzero, reducing K_1^v below the shape anisotropy energy $2\pi M_s^2$, *does not* make the easy axis fall abruptly in the plane of the sample. The easy cone of magnetization rather opens progressively, making an angle $\theta=\arcsin[(2\pi M_S^2-K_1^v)/2K_2]$ with the normal of the surface. This is the case for the three irradiated areas.

The spectroscopic dependence of the Kerr signals (not shown) exhibits no feature characteristic of local chemical ordering.[28] The Kerr rotation increases slightly in the far UV spectrum and significantly for wavelength $\lambda>310-340$ nm. The Kerr ellipticity increases at all wavelengths. Such an

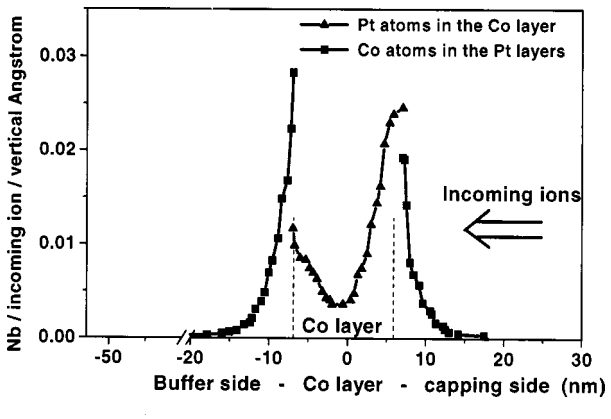

FIG. 5. Distribution of foreign atoms in an irradiated Pt/Co (13 Å)/Pt structure, i.e., cobat atoms (squares) in the buffer and capping layers and platinum atoms (triangles) in the nominal Co layer. TRIM simulation after 8×10^5 incoming ions.

evolution is similar to that observed in disordered Co-Pt alloys when increasing both the Pt composition and the total magnetic alloy thickness.[29]

IV. DISCUSSION

We shall first compare our experimental trends to purely collisional mixing simulations and see whether the main structural evolutions—the nonsymmetric roughness, the mixing ranges, and rates—are compatible with this simple model. Keeping in mind that GXR is not sensitive to grain size, order/disorder effects, and crystalline structure, we shall then address the correlation between magnetic and structural properties and, in particular, discuss the magnetic anisotropy decrease.

A. Ballistic recoil mechanism of mixing

We have performed TRIM (Ref. 12) simulations on a perfect sandwich Pt(41 Å)/Co(13 Å)/Pt(22 Å), with initially pure layers in order to simulate[30] the first stages of ion beam mixing. Figure 5 shows the distribution of foreign atoms, i.e., Co atoms knocked in the Pt buffer or in the Pt cap layers or Pt atoms kicked inside the Co layer. Note that there are 40% more Pt atoms knocked into the Co layer than Co atoms knocked into the Pt layers. This implies that immediately after irradiation (before any diffusion or recombination process) the atomic density of the different layers has changed. When multiplying the simulated implantation rate by a fluence of 10^{16} ions/cm^2, the resulting maximum foreign atom local concentration is 38%. The probability for a given atom to undergo two He^+ collisions is thus everywhere lower than $0.38^2=14\%$ at $F=10^{16}$ ions/cm^2. As a result, the two lower fluences belong to the quasilinear mixing regime where the likelihood for a given atom to undergo two collisions with He ions is still low. Conversely, the highest fluence belongs to the cumulative mixing regime, so that the calculated concentration shall only be considered as indicative.

The calculated foreign atom distribution gives three major pieces of information: (i) the characteristic lengths of the problem, (ii) the mixing rates, and (iii) an insight into sandwich roughness asymmetry.

1. Characteristic dimensions

The characteristic lengths of the mixing process are summarized in Table II.

In Fig. 5, the distributions of Co atoms under or over the Co layer fall off exponentially away from the initial interfaces with characteristic decay ranges of, respectively, 2.7 and 1.5 Å. The Pt distribution is smoother: the typical decay lengths are ~4.5 Å on both cap and buffer side, so that the Pt concentration is nonzero in the center of the Co layer. These numbers integrate all events weighted by their respective probability. They are related to the most probable range of a given atom after a 30-keV He^+ ion collision. The mean transferred energy in a He-Co (respectively, He-Pt) collision is 85 eV (respectively, 68 eV). The corresponding path of 85 eV Co in a Pt layer is 3 Å, whereas that of 68 eV Pt in a Co layer is 5 Å.[12] In summary, Pt atoms penetrate deeper in the Co layer than Co atoms do in the Pt layers; as a result, the Pt concentration gradient inside the Co layer is less abrupt than that of Co in Pt.

Thanks to the momentum conservation during collision, Co atoms are mainly driven inwards the buffer, whereas Pt cap atoms are driven into the upper part of the cobalt layer. Secondary collisions may occur: an already knocked atom can collide one of its neighbors. Sometimes, it makes an atom travel towards the surface (backwards the ion direction). Such a secondary process in the backward direction is rare and of low energy, so that there is a high asymmetry between Co concentration decay rates over and under the cobalt layer.

The ranges of Table II are consistent with a rapid decrease of the 5-Å Pt underlayer index and a slower decreasing rate for the Pt overlayer. In addition, because the calculated penetration of Co in Pt is small, the index of the two Pt layers that are far away from the Co layer should be stable, at least in the quasilinear mixing regime.

2. Mixing rates

The mean calculated foreign atom concentrations are given in Table III between square brackets. In order to com-

TABLE II. Characteristic lengths of the irradiation-induced mixing process.

Most probable range (Å)			Characteristic extension of the concentration gradient projected on Pt[111] (Å)		
Pt atom in Co matrix	Co atom inwards in Pt underlayer	Co backwards in Pt overlayer	Pt atom in Co matrix	Co atom inwards in Pt underlayer	Co backwards in Pt overlayer
5 Å	3 Å	Secondary collision only	4.5 Å	2.7 Å	1.5 Å

TABLE III. Comparison between the experimental foreign atoms concentrations determined by GXR and by mixing simulations for a Pt/Pt(5 Å)/Co(13 Å)/Pt(5 Å)/Pt sandwich. The simulation data are given between square brackets. Experimental determination of mixing rate in the Pt overlayer is prevented by its competition with strain release.

Fluence:	6×10^{15} ions/cm^2		10^{16} ions/cm^2		3×10^{16} ions/cm^2	
Co in Pt underlayer	3.6%	[6.4%]	4.4%	[10.8%]	12.4%	[<32%]
Pt atoms in Co layer	3.5%	[7%]	7%	[11%]	19%	[<34%]
Co in Pt overlayer	Stress release regime	[3.8%]	Stress release regime	[6.3%]	>1.5%	[<18.8%]

pare them with the GXR data, we estimated the experimental foreign atom concentration $[x]$ using a simple Vegard assumption,

$$\delta_{\mathrm{exp}}=[x]\delta_{\mathrm{Co}}+(1-[x])\delta_{\mathrm{Pt}}, \tag{4}$$

and our experimental Co and Pt indices found for zero fluence. This is crude estimate since it neglects any possible change of atomic density and assumes flat interfaces.

The data collected in Table III indicate that the order of magnitude of Pt implantation into Co is correct. Simulation seems to overestimate all the implantation rates by ~80%. In view of the approximations made above, this agreement may be regarded as satisfactory.

Experiments and calculations agree that the Pt underlayer and the Pt buffer behave differently: the incorporation of Co into Pt has a range smaller than 5 Å. The characteristic lengths displayed in Table II are thus relevant quantities.

Finally, the asymmetry in alloy concentrations over and under the central layer is also concluded from the two methods. This provides a strong indication that the mixing effect is largely driven by a collisional mechanism.

The evolution of the index of the Pt overlayer, which first increases and then decreases, and the increase of Pt buffer and cap refractive indices could be due to the increase of atomic density due to a decrease of the lattice unit cell volume. Large modifications of interatomic distances were observed for 60-keV He^+ irradiation of Cu/W superlattices.[31] In our case, the strain change would occur similarly in all Pt layers, but its observation would be hindered in the Pt underlayer because of the high Co implantation rate. As seen from Fig. 3, the Pt layer densification slows down for the highest fluences (see, for instance, the variation of the refraction index of the Pt cap layer, a layer which is out of reach of the knocked Co atoms).

Since the coherence length along Pt[111] is the full sandwich thickness, the unit cell volume reduction should also occur inside the Co layer. Preliminary extended x-ray absorption fine spectroscopy (EXAFS) analysis[32] at the Co edge confirms a 6% reduction of the unit cell volume around a cobalt atoms. The change of the in-plane parameter is −3.3%.

Adding this effect in Eq. (4) would lower the GXR-estimated incorporation rate of Pt into cobalt and would increase the GXR-estimated incorporation rate of Co into the Pt underlayer. A better agreement between collisional mixing and GXR data would be attained for incorporation rate of Co into the Pt underlayer. A worse agreement between collisional mixing and GXR data would be attained for incorporation rate of Pt cap atoms into the Co layer.

3. Sandwich roughness asymmetry

The number of foreign atoms is maximum near the interfaces: this will affect interface roughness. rms roughness can unfortunately not be computed within our model. To discuss the alloying effect, we have estimated the number of foreign atoms in each entire layer. To discuss the roughness values, we shall now calculate the proportion of foreign atoms located closer than 3 Å apart from a given interface.[33] From Fig. 5, this proportion of foreign atoms near the lower Co interface is 36% for a fluence of 10^{16} ions/cm^2 and is 1.4 times more near the upper Co interface. Qualitatively, the Co atoms knocked towards the substrate side travel far enough so that alloy formation may be assumed, whereas the Co atoms knocked towards the surface side through secondary collisions travel at lower distances and stay in direct contact with the Co layer, so that a roughness increase is triggered. A schematic of this scenario is displayed on Fig. 6.

However, the ballistic recoil mechanism cannot account exactly for the experimental asymmetry between upper and lower Co/Pt interface's roughness, between which there is a factor of 2 instead of 1.4. Just as it was the case for the mixing rate, it now seems that Co atoms enter in Pt as easily as predicted by purely collisional mixing, whereas Pt atoms do not manage to enter the Co layer as easily as they should. This could be due to a nonsymmetrical chemical potential

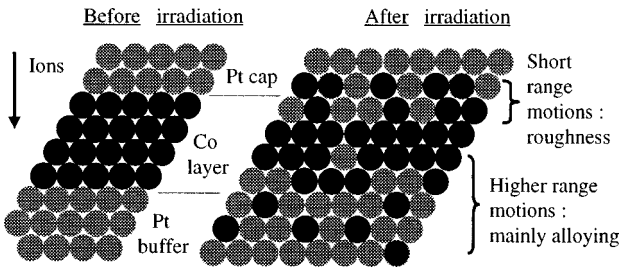

FIG. 6. Qualitative schematic of a sandwich structure before and after irradiation. Co (Pt, respectively) atoms are in black (respectively, gray). Ions move towards the bottom of the figure. Co atoms moving in the ion direction travel more than one interatomic distance and become isolated (Co-Pt alloying), whereas Co atom moving in the opposite direction travel typically only one interatomic distance and contribute to roughness (local thickness fluctuations).

gradient, the role of thermodynamics being to stabilize[34] the Co atoms transported in the Pt fcc matrix (alloy formation) rather than[35] the Pt atoms inside the Co hcp layer (segregation resulting in roughness). This illustrates why ion-induced modifications are rather stable versus annealing at 200 °C (Ref. 7) in our miscible systems. This is not the case with strongly immiscible systems such as Fe/Ag multilayers, where annealing allows recovery of abrupt interfaces.[36] This specificity of hcp-Co/fcc-Pt chemistry can enhance the asymmetry between upper and lower Co interface structure sketched in Fig. 6.

In summary, a purely ballistic model can semiquantitatively account for the different mixing rates, their range in Pt and Co, and the roughness asymmetry of the Co layer. This further supports the conclusions drawn by the structural studies of Sec. III A. Thermodynamical effects should be taken into account for a more precise description of the mixing. Finally, to explain the mean refractive index global increase, we conjecture a reduction of the crystal lattice unit cell volume in the whole metallic thickness.

B. Correlation between structure and magnetic anisotropy

The evolution of magnetic anisotropy can either stem from volume effects or interface effects.[1]

The anisotropy contributions proportional to the magnetic volume are shape anisotropy, magnetocrystalline anisotropy and magnetoelastic anisotropy.

(i) Shape anisotropy is constant because saturation magnetization M_S is.

(ii) While randomly incorporating Pt into bulk Co, the magnetocrystalline contribution can decrease from 4.5×10^6 erg/cm^3 (pure hcp Co) to ~ 0 (random fcc Co-Pt alloy). If the Pt incorporation was performed together with a local chemical ordering, the magnetocrystalline anisotropy would drastically increase.[28] It has been shown recently that 130-keV He^+ irradiation at higher temperature (280 °C) can induced partial chemical ordering of FePt.[37] Here spectroscopic PMOKE measurements do not exhibit the spectral signatures[28] of chemical ordering when irradiating Co/Pt at room temperature, so that magnetocrystalline anisotropy should decrease with the Pt concentration inside the Co layer.

(iii) Thanks to the lattice mismatch between Pt and Co, the as-deposited Co layer is in tensile stress. We have shown that the Pt layer densification could be interpreted in terms of strain relaxation. We have conjectured a decrease of the lattice unit cell volume in both Pt and Co layers. Our GXR experiments can unfortunately not distinguish between Pt enriching of the Co layer and strain relaxation within it. We have shown in the previous section that both are very likely to happen. EXAFS measurements are in progress[32] to further characterize these two rates. However, the magnetoelastic anisotropy of Co is negative. Thus, if the Co layer tensile stress is reduced, PMA is lowered. Note that the strain release rate is the only structural parameter that does not vary linearly with the fluence.

In the absence of interface anisotropy, the easy axis of magnetization would be in plane for all layer thicknesses and irradiation fluences. The more abrupt the interfaces are, the higher the (interface) anisotropy.[38] Hence irradiation should lower the interface anisotropy. Such a decrease should scale with the roughness evolution, which is linear with regards to the fluence (Fig. 2). Note, however, that only the upper interface roughness is affected by irradiation, so that the contribution of each interface should not be altered the same way; the interface contribution to the total magnetic anisotropy cannot be reduced by more than a factor of 2.

In the case of thinner (5 Å of Co) Ref. 7 sandwiches or multilayers,[5,19] it has been reported that the irradiation-induced decrease of anisotropy is linear. These ultrathin Co layers comprise only Co atoms located at an interface, so that the decrease of anisotropy could almost exclusively be ascribed to the roughening of the interfaces. In addition, only low fluences were considered.

A high fluences, the decrease of anisotropy is not linear: it starts abruptly and then slows down, because several structural phenomena are involved. We have shown that the strain relaxation is the main phenomenon at intermediate and low fluences while mixing process becomes dominant at moderate and high fluences, when the strain relaxation rate slows down. This explains the evolution of the Co sandwich anisotropy.

K_1^v decreases first because of combined strain relaxation in the Co layer and upper interface roughening. Then, when stress is relaxed, only the roughening of the upper Co/Pt interface decreases the magnetic anisotropy. Since K_2^v is a purely volume contribution, it is mainly affected in the strain relaxation regime, e.g., at low fluences.

V. CONCLUSION

Finally, light ion irradiation is a powerful tool to tune magnetic properties without affecting planarity.[5] This technology is compatible with mass production standards,[19] and has proven sub-50-nm resolution.[8,9]

Purely ballistic recoil processes can rather accurately explain most of the mixing characteristics of 30-keV He^+ irradiation of Pt/Co/Pt sandwiches. Simulation confirm the structural trends determined by GXR: even in these nm-thick sandwiches, irradiation does not affect in the same way the upper and lower interfaces. More precisely, the upper interface is mainly affected by short-range atomic motions generating roughness (Co thickness local fluctuations), whereas atoms near the lower interface undergo higher-range motions, resulting in alloy formation. Grazing x-ray reflectometry also indicates an irradiation-induced densification of the metallic layers. To account for this, we conjecture that irradiation helps to release strain. Although no chemical ordering is involved during irradiation, full understanding of the irradiation-induced structural changes would require implementation of thermodynamics of binary Co_xPt_{1-x} alloy systems into the structural model.

Our magnetic results indicate that the decrease of magnetic anisotropy may be related to two phenomena. At relatively low fluences ($F \leqslant 10^{16}$ He^+/cm^2) irradiation triggers cobalt strain release and thus reduces the magnetoelastic contribution to magnetic anisotropy. At the same time, the upper interface roughness increase linearly with the irradiation fluence. This linearly lowers the interfacial contribution to perpendicular magnetic anisotropy. This scenario—strain relax-

ation and asymmetric mixing—can be generalized to any Co/Pt system; for very thin Co layers, only the interface roughness anisotropy term should vary. Our analysis bears on previous reports[7,10] concerning the variation of the magnetic anisotropy with the irradiation fluence and opens the route to understand light ion modification of other magnetic properties, such as interlayer exchange coupling.[13]

ACKNOWLEDGMENTS

The author acknowledges V. Mathet for sample preparation; he is grateful to H. Bernas for very helpful discussions on irradiation effects and modeling. He also acknowledges D. Ravelosona and C. Chappert for interesting discussions on GXR sensitivity.

*Fax: (33) 1 69 15 40 00. Email address: devolder@ief.u-psud.fr

[1] P. Bruno, *Magnetismus von Festkörper und Grenzflächen* (Ferienkurse des Forschungszentrums Jülich, Jülich, Germany, 1993), Chap. 24.

[2] M. Mansuripur, *The Physical Principles of Magneto-Optical Recording* (Cambridge University Press, Cambridge, England, 1995).

[3] For a review, see the Proceedings of the 4th Perpendicular Magnetic Recording Conference [J. Magn. Soc. Jpn. **21**, S2 (1997)].

[4] D. Weller, H. Brändle, G. Norman, C.-J. Lin, and H. Notarys, Appl. Phys. Lett. **61**, 2726 (1992).

[5] C. Chappert, H. Bernas, J. Ferré, V. Kottler, J. P. Jamet, Y. Chen, E. Cambril, T. Devolder, F. Rousseaux, V. Mathet, and H. Launois, Science **280**, 1919 (1998).

[6] M. G. Le Boité, A. Traverse, L. Névot, B. Pardo, and J. Corno, J. Mater. Res. **3**, 1089 (1988); M. G. Le Boité, A. Traverse, H. Bernas, C. Janot, and J. Chevrier, J. Mater. Sci. Lett. **6**, 173 (1988); A. Traverse, M. G. Le Boité, and G. Martin, Europhys. Lett. **8**, 633 (1989).

[7] J. Ferré, C. Chappert, H. Bernas, J.-P. Jamet, P. Meyer, O. Kaitanov, S. Lemerle, V. Mathet, F. Rousseaux, and H. Launois, J. Magn. Magn. Mater. **198–199**, 191 (1999).

[8] T. Devolder, C. Chappert, Y. Chen, E. Cambril, H. Bernas, J.-P. Jamet, and J. Ferré, Appl. Phys. Lett. **74**, 3383 (1999).

[9] T. Devolder, Y. Chen, C. Chappert, H. Bernas, J. Ferré, J. P. Jamet, E. Cambril, and H. Launois, J. Vac. Sci. Technol. B **37**, 3117 (1999).

[10] T. Aign, P. Meyer, S. Lemerle, J. P. Jamet, J. Ferré, V. Mathet, C. Chappert, J. Gierak, C. Vieu, F. Rousseaux, H. Launois, and H. Bernas, Phys. Rev. Lett. **81**, 5656 (1998).

[11] S. Y. Chou, Proc. IEEE **85**, 652 (1997).

[12] J. Ziegler, J. Biersack, and U. Littmark, *The Stopping of Ions in Matter* (Pergamon, New York, 1985).

[13] T. Mewes, R. Lopusnik, J. Fassbender, B. Hillebrands, M. Jung, D. Engel, A. Ehresmann, and H. Schmoranzer, Appl. Phys. Lett. **76**, 1057 (2000).

[14] C. Mény and P. Panissod (private communication).

[15] J. Chaumont, F. Lalu, M. Salomé, A. M. Lamoise, and H. Bernas, Nucl. Instrum. Methods Phys. Res. **189**, 193 (1981).

[16] The Cu $K\beta$ radiation was eliminated with a nickel filter.

[17] C. Train, P. Beauvillain, V. Mathet, G. Pénissard, and P. Veillet, J. Appl. Phys. **86**, 1 (1999).

[18] H. Kiessig, Ann. Phys. (Leipzig) **10**, 715 (1931).

[19] B. D. Terris, L. Folks, D. Weller, J. E. E. Baglin, A. J. Kellock, H. Rothuizen, and P. Vettiger, Appl. Phys. Lett. **75**, 403 (1999).

[20] A. Guinier, *Théorie et Technique de la Radiocristallographie* (Dunod, Paris, 1964), p. 462.

[21] L. G. Parratt, Phys. Rev. **95**, 359 (1954).

[22] L. Névot, Acta Electron. **24**, 255 (1982); X. L. Zhou and S. H. Chen, Phys. Rep. **257**, 223 (1995).

[23] The roughness of the initial surface consists of 5–10 nm terraces separated by monoatomic steps; from L. Belliard (private communication). The grain size determined by AFM is 30–40 nm and does not seem to vary with the irradiation fluence.

[24] While writing this manuscript, the author was informed about a similar effect for FePt sandwiched between two Pt layers submitted to 130-keV He^+ irradiation [D. Ravelosona (private communication)].

[25] We considered that a χ^2 test equal to 5 is the best achievable (noise-limited theory/experiment agreement). Slight differences appear when $\chi^2>5$, and some of them become very clear when $\chi^2>10$. Starting with pure and flat layers gave a typical χ^2 of 65.

[26] Dividing the cap into two sublayers is a way to probe the Co concentration gradient. We shall see in the following sections that this gradient is very low and that the cap layer is very homogeneous. Thus choosing a thicker or a thinner Pt overlayer will not affect the experiment-fit agreement.

[27] L. Cagnon, T. Devolder, R. Cortes, A. Morrone, J. Schmidt, C. Chappert, and P. Allongue (unpublished).

[28] (i) For Co_3Pt, a K_1^v of -2×10^7 erg/cm^3 and a maximum of Kerr rotation at 3.2 eV (387 nm) was found by G. R. Harp, D. Weller, T. A. Rabedeau, R. F. C. Farrow, and M. F. Toney, Phys. Rev. Lett. **79**, 5290 (1997) and G. Lauhoff, Y. Yamada, Y. Itoh, and T. Suzuki, in Proceedings of Magneto-Optical Recording International Symposium 99 [J. Magn. Soc. Jpn. **23**, s1-43 (1999)]. (ii) For CoPt, G. R. Harp, D. Weller, T. A. Rabedeau, R. F. C. Farrow, and R. F. Marks, in *Magnetic Ultrathin Film—Multilayers and Surfaces, Interfaces and Characterization*, edited by B. T. Jonker *et al.*, MRS Symposia Proceedings No. 313 (Materials Research Society, Pittsburgh, 1993), p. 493, reported a strong peak at 2.2 eV in the Kerr rotation spectrum. (iii) For $CoPt_3$, R. J. Lange, S. J. Lee, D. W. Lynch, P. C. Canfield, B. N. Harmon, and S. Zollner, Phys. Rev. B **58**, 351 (1998), have demonstrated that both Kerr rotation and ellipticity exhibit a peak structure between 2.0 and 2.3 eV; M. Maret, M. C. Cadeville, W. Staiger, E. Beaurepaire, R. Poinsot, and A. Herr, Thin Solid Films **275**, 224 (1996), have reported K_1^v up to 10^7 erg/cm^3.

[29] The Kerr spectra of disordered Co_xPt_{1-x} alloys can be found, for instance, in H. Brändle, D. Weller, J. C. Scott, S. S. P. Parkin, and J. C. Lin, IEEE Trans. Magn. **28**, 2967 (1992).

[30] TRIM Monte Carlo simulations account for ion-atom collisions in a full quantum mechanical treatment. During the collisions, the ion and atom have a screened Coulomb interaction, including exchange and correlation between the overlapping electron shells. Its two-body collision approximation is particularly accurate in the case of light ion irradiation. Successive ion collisions are treated as independent.

[31] J. Pacaud, G. Gladyszewski, C. Jaouen, A. Naudon, Ph. Goudeau, and J. Grilhé, J. Appl. Phys. **73**, 2786 (1993).

[32] T. Devolder, H. Bernas, D. Ravelosona, C. Chappert, S. Pizzini, J. Ferré, J. P. Jamet, Y. Chen, and V. Mathet (unpublished).

[33] The value of 3 Å was chosen because it is near the roughness of

the as-deposited Co interfaces. Making the same evaluation with 2 or 4 Å does not change significantly the conclusions we draw.

[34] J. M. Sanchez, J. L. Moran-Lopez, C. Leroux, and M. C. Cadeville, J. Phys. C **21**, 1091 (1988).

[35] At 300 °C, the maximum stable concentration of Pt in hcp Co is ~15%, whereas the maximum amount of Co in fcc Pt is more than 60% (no data available at room temperature because of kinetic limitations), from T. B. Massalski, *Binary Alloy Phase Diagrams*, 2nd ed. (Metal Information Society, Metals Park, OH, 1990).

[36] D. Kurowski, K. Brand, and J. Pelzl, Nucl. Instrum. Methods Phys. Res. B **148**, 936 (1999).

[37] D. Ravelosona, C. Chappert, V. Mathet, and H. Bernas, Appl. Phys. Lett. **76**, 236 (2000).

[38] G. A. Bertero, R. Sinclair, C.-H. Park, and Z. X. Shen, J. Appl. Phys. **77**, 3953 (1995).